

An extensive comparison of anisotropies in MBE grown (Ga,Mn)As material.

C Gould¹, S Mark¹, K Pappert¹, G Dengel¹, J Wenisch¹, R P
Campion², A W Rushforth², D Chiba^{4,5}, Z Li³, X Liu⁶, W Van
Roy³, H Ohno^{5,4}, J K Furdyna⁶, B Gallagher², K Brunner¹, G
Schmidt¹, L W Molenkamp¹

¹Physikalisches Institut (EP3), Universität Würzburg, Am Hubland, D-97074
Würzburg, Germany

²School of Physics and Astronomy, University of Nottingham, Nottingham NG7
2RD, United Kingdom

³IMEC, Kapeldreef 75, B-3001 Leuven, Belgium

⁴Semiconductor Spintronics Project, Exploratory Research for Advanced Technology,
Japan Science and Technology Agency, Kitamemachi 1-18, Aoba-ku, Sendai
980-0023, Japan

⁵Laboratory for Nanoelectronics and Spintronics, Research Institute of Electrical
Communication, Tohoku University, Katahira 2-1-1, Aoba-ku, Sendai 980-8577,
Japan

⁶Department of Physics, University of Notre Dame, Notre Dame, Indiana 46556, USA

E-mail: gould@physik.uni-wuerzburg.de

Abstract.

This paper reports on a detailed magnetotransport investigation of the magnetic anisotropies of (Ga,Mn)As layers produced by various sources worldwide. Using anisotropy fingerprints to identify contributions of the various higher order anisotropy terms, we show that the presence of both a [100] and a [110] uniaxial anisotropy in addition to the primary ([100] + [010]) anisotropy is common to all medium doped (Ga,Mn)As layers typically used in transport measurement, with the amplitude of these uniaxial terms being characteristic of the individual layers.

PACS numbers: 75.50.Pp, 75.30.Gw, 85.75.-d

1. Introduction

A key prototypical material for investigations into spintronics is the ferromagnetic semiconductor (Ga,Mn)As. The marriage of magnetic and semiconductor properties brought about by strong spin-orbit coupling, which ties the density of states of this material to its magnetic properties, offers a host of new and exploitable magnetotransport effects. As investigations into this material continue to progress, it has become clear that a detailed understanding of the underlying magnetic anisotropy is a key issue in device design and optimization.

This magnetic anisotropy in (Ga,Mn)As is very rich and complicated, which led to various reports over the past decade which superficially appeared to be contradictory. In general, depending on growth strain, doping density and temperature, the material can have an easy axis of magnetization either perpendicular to plane, or in the layer plane [1, 2], and in the latter case, the primary anisotropy can be either biaxial along [100] and [010], or uniaxial along either [110] or $\bar{1}10$ [3, 4].

It is generally accepted that for typical medium doped transport samples with ~ 3 to 6 % Mn, grown with compressive strain and measured at 4 K, the primary anisotropy is a biaxial term with easy axes along the [100] and [010] crystal directions. Second order terms are also widely reported in the form of a uniaxial easy axis along [110] or $\bar{1}10$ [5] of various relative strengths, or a uniaxial along [010] [6].

Since it is well known in the community that the detailed properties of (Ga,Mn)As depend on exact growth conditions such as substrate temperature, growth rate, flux ratios, etc. [7, 8, 9], it was initially widely assumed that the observation of these different higher order anisotropy terms were primarily a result of the distinct properties of the various layers used.

It is now realized that part of the confusion arose from the fact that the various transport measurement from which these terms had been extracted differ in sensitivity to the different anisotropy terms. For example, in the non-volatile Tunneling Anisotropic Magnetoresistance (TAMR) experiments [6], the [010] plays a crucial role whereas the [110] anisotropy is nearly irrelevant because it only has significant impact for volatile effects occurring at higher fields. On the other hand, the [010] term plays only a secondary role in the planar Hall measurements of hall bars along the [110] direction [5].

Moreover, because these second order uniaxial anisotropy terms are significantly weaker than the primary biaxial anisotropy, they cannot be reliably characterized by direct magnetization measurements such as SQUID (Superconducting Quantum Interference Device) or VSM (Vibrating Sample Magnetometer). The challenge of fully characterizing the complex anisotropies in (Ga,Mn)As was recently successfully addressed with the development of an "anisotropy fingerprint" technique [10] which consists of taking magnetotransport measurements for magnetic fields swept in multiple directions.

Using this method, we recently investigated [11] various transport samples produced

on wafers grown in a given Molecular Beam Epitaxy (MBE) system at Würzburg University, and showed that in all cases, a detailed investigation revealed the presence of both [010] and [110] uniaxial terms, with the sign and relative amplitude of these two terms varying from sample to sample. In the present paper, we expand this investigation to samples grown by multiple groups and show that indeed the co-existence of all anisotropy terms is a general property of (Ga,Mn)As, and that only the relative strength of the terms is characteristic of the layer growth.

2. Anisotropy fingerprints

All investigations are performed using Hall bars of the configuration shown in Fig. 1a produced by standard optical lithography followed by chemically assisted ion beam etching (CAIBE). Magnetoresistance measurements are carried out in a magnetocryostat equipped with a vector field magnet capable of producing fields of up to 300 mT in any spatial direction. For the measurement discussed in this paper, fields are always applied in the plane of the sample, and the direction of the magnetic field is given by the angle ϕ relative to the [100] crystal direction.

(Ga,Mn)As exhibits a strongly anisotropic magnetoresistance (AMR) where the resistivity ρ_{\perp} for current flowing perpendicular to the direction of magnetization is larger than ρ_{\parallel} for current along the magnetization [12]. As a result of this anisotropy in the resistivity tensor, the longitudinal resistivity ρ_{xx} is given by [13, 14]:

$$\rho_{xx} = \rho_{\perp} - (\rho_{\perp} - \rho_{\parallel}) \cos^2(\vartheta), \quad (1)$$

where ϑ is the angle between the direction of magnetization and the current. Note that there is also a dependence of the resistivity on the angle between the direction of magnetization and the underlying crystal orientation [15]. This additional term modifies the resistivity value for a given magnetization directions, but does not effect the field position of the magnetization reorientation events, and can thus be neglected for the purposes of the present analysis.

For each sample, we measure the four terminal longitudinal resistance using the lead configuration given in Fig. 1a by passing a current from the I_+ to the I_- contacts, and measuring the voltage between V_1 and V_2 . We scan the magnetic field from -300 mT to +300 mT along a given direction ϕ , and repeat this procedure for multiple angles. A simulation of such a scan for the case of $\phi = 70^\circ$ is given in Fig. 1c, and shows two switching events, labeled H_{c1} and H_{c2} associated with the two sequential 90° domain wall nucleation/propagation events which account for the magnetization reversal in this material [16]. In order to analyze the data, the positive field half of each of these scans are converted to a sector of a polar plot as shown in Fig. 1d. The two switching events then show up as abrupt color changes as indicated in the figure. The compilation of all the sectors required for a full revolution produces an anisotropy fingerprint resistance polar plot as the one simulated in Fig. 2a.

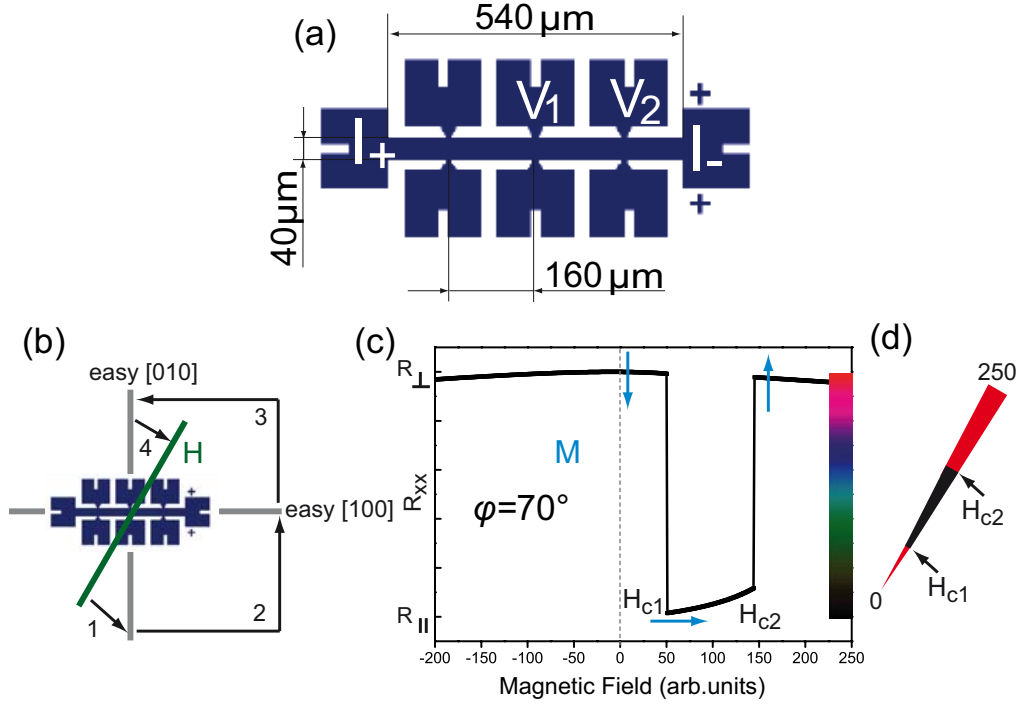


Figure 1. *a: Layout of the Hall bar used in the experiments. b: Configuration for the simulation of a magnetoresistance scan along $\phi = 70^\circ$ (c) showing the two switching event H_{c1} and H_{c2} corresponding to the two subsequent 90° domain wall propagation events. This data is then converted (d) to a sector of a resistance polar plot.*

For the purposes of characterizing the various anisotropy terms, the most important part of the data is the innermost region whose boundaries are formed by the loci of first switching events (H_{c1}). Fig. 2b shows a zoomed in view of this region for an experimental measurement on a characteristic piece of (Ga,Mn)As.

For the model case of a purely biaxial anisotropy, this inner region would take the form of a perfect square with corners along the easy axis and the length of the half diagonal given by ε/M , the domain wall nucleation/propagation energy scales to the volume magnetization (Fig. 3a). The inclusion of a uniaxial anisotropy bisecting two of the biaxial easy axes moves the resulting easy axes towards the direction of the uniaxial anisotropy [17] and elongates the square into a rectangle as schematically depicted in Fig. 3b. The strength of the uniaxial anisotropy constant in the $[110]$ direction K_{110} relative to the biaxial anisotropy constant K_{biax} can be extracted from the angle δ , as defined in Fig. 3b, by which the angle between two easy-axes is modified. The relationship is given by [11]:

$$\delta = \arcsin \left(\frac{K_{uni[110]}}{K_{biax}} \right) \quad (2)$$

In practice, because the mixing of the anisotropy terms leads to a rectangle with open corners, it is often more convenient to work with the aspect ratio of the width

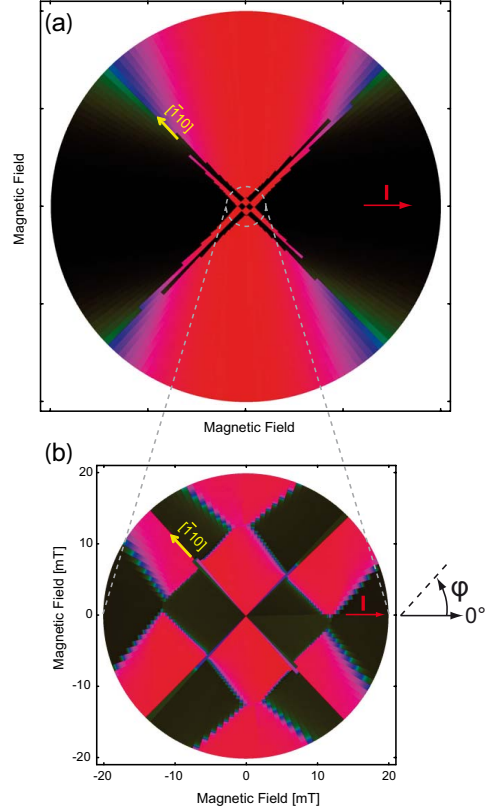


Figure 2. *a: Simulation of a full resistance polar plot comprised of sectors as in Fig. 1. b: measurement of the inner region of the polar plot. The red I indicates the direction of current flow during the measurement.*

(W) to the length (L) of the rectangle, instead of the angle δ , which is related to the anisotropy terms as:

$$\frac{K_{uni[110]}}{K_{biax}} = \cos \left(2 \arctan \left(\frac{W}{L} \right) \right) \quad (3)$$

If a uniaxial anisotropy is instead added parallel to one of the biaxial easy axes, an asymmetry arises in the energy required to switch between the two biaxial easy axes. Essentially, the energy required to switch towards the easier of the two biaxial easy axis is less than that to switch towards the second biaxial. The inner pattern is then comprised of parts of an inner and an outer square, and the difference in the length of their half diagonal is a measure of K_{010} (Fig. 3c), where K_{010} is the [010] anisotropy constant. Because of deformation of the fingerprint near the corners of the rectangle, which results from mixing of the anisotropy terms, it is often easier to identify the presence of an [010] uniaxial easy axis by looking at the spacing between the sides of the squares (or rectangles in the case that a [110] uniaxial term is also present), as indicated by the yellow line in Fig. 3c, which of course has a length equal to $\sqrt{2}K_{010}$

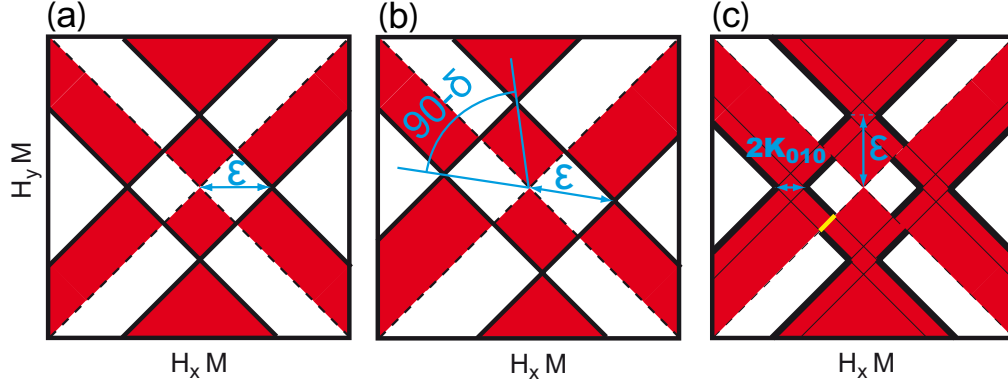


Figure 3. Sketches of the expected shape of the inner region for a) a samples with only a $([100]$ and $[010])$ biaxial anisotropy. b) a sample with a biaxial plus a $[\bar{1}10]$ uniaxial easy axis, and c) a samples with a biaxial plus a $[010]$ uniaxial easy axis. Note that the axis are in magnetic field units scaled to the volume magnetization (M).

3. Characteristic of a wafer

We have previously shown [11] that the fingerprint technique can be used to characterize the properties of a given wafer, and for macroscopic sized devices the fingerprint is a signature of the underlying material. As an example of this, we present in Fig. 4 the fingerprints for two Hall bars patterned from different locations on the same (Ga,Mn)As wafer, and oriented orthogonal to each other. An inspection of both fingerprints shows that the pattern is identical, as would be expected from an homogenous wafer. The colors are inverted because of the 90° difference in current orientation. Both fingerprints yield the values of 1 mT for K_{010}/M , 18 % for K_{110}/K_{biax} and 18 mT for ϵ/M .

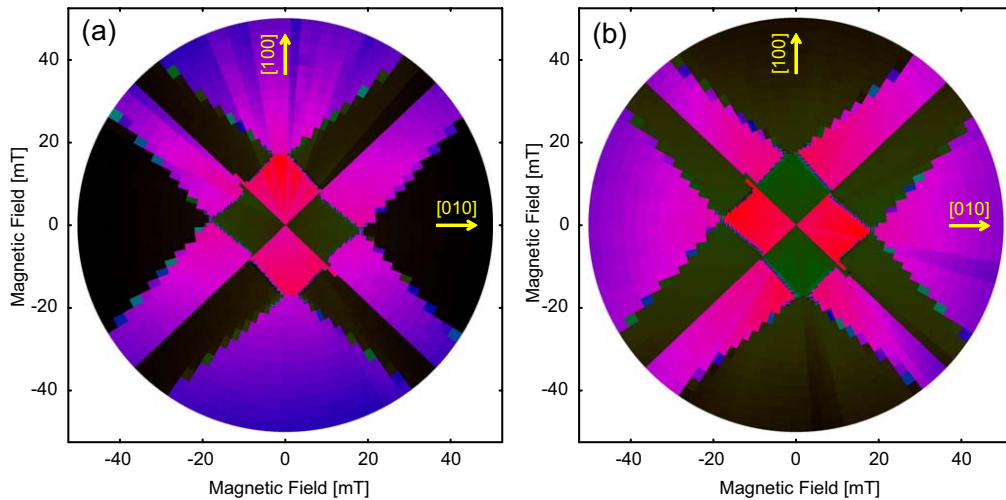


Figure 4. Resistance polar plots taken on two different locations of the same (Ga,Mn)As layer.

Next, we demonstrate how this technique can be used also as quality control process. Figure 5 shows 3 fingerprints from three pieces of the same (Ga,Mn)As layer, taken near

the center of the 2 inch wafer, and 4 and 1 mm from the edge. Because of the geometry of the Würzburg MBE chamber, and given that the substrate is rotated during growth to enhance radial homogeneity, the uniformity of the sample is nearly perfect near the center and any fingerprint taken in that region is identical to that of Fig. 5a. From the figure we see that the central part of the sample has rather typical values of 16 % for K_{110}/K_{biax} , 0.7 mT for K_{010}/M , and 9.2 mT for ϵ/M . Because of non-linearities in the molecular beam profile, stoichiometric deviations in the epilayer become significant near the edge of the wafer. The outermost 5 mm of samples are thus significantly less uniform. This area is normally discarded, and certainly not used for device studies. The fingerprint in Fig. 5c, taken on a piece 1 mm from the edge very clearly shows why. It presents a fingerprint pattern very different from the homogenous center, with an enormous discontinuity in the edges of the squares corresponding to a very large value of $K_{010}/M = 3.8$ mT for the [010] uniaxial anisotropy term. This is well outside the range of what is found on the homogeneous part of any (Ga,Mn)As. The deformation is sufficient that it is impossible to reliably extract values K_{110} or ϵ . The fingerprint of Fig. 5b, on a piece 4 mm from the edge, is just outside the region that is normally considered usable. It has approximately the same value of ϵ and K_{010} as the central part and is only slightly deformed with a smaller K_{110}/K_{biax} of 12%. These numbers are still within the typical range for (Ga,Mn)As, but show a change in layer properties as one approaches the edge.

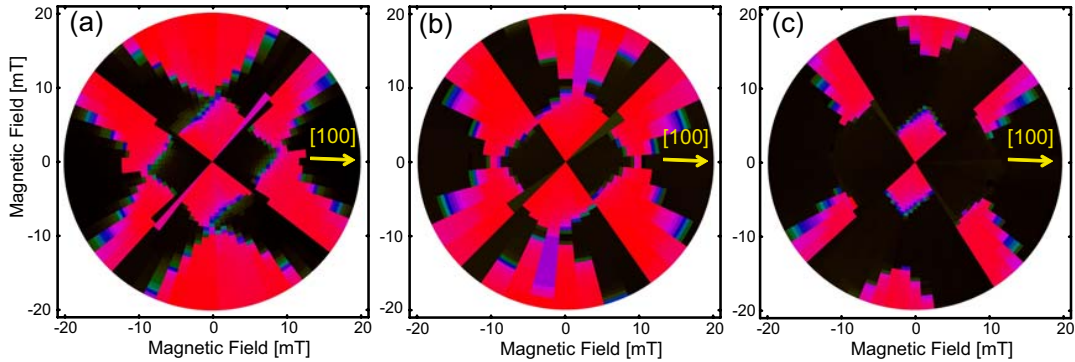


Figure 5. Resistance polar plots taken a) near the center of a (Ga,Mn)As wafer, b) about 4 mm from the edge of the wafer, and c) about 1 mm from the edge.

4. Comparison of wafers from multiple sources

In order to confirm that the coexistence of both the [010] and [110] uniaxial anisotropy terms are not a particularity of (Ga,Mn)As grown in a certain MBE chamber or under particular conditions, but are indeed ubiquitous to the material, we now present the results of measurements performed on samples patterned from layers grown in various laboratories and thus under varied growth conditions.

Figure 4 showed fingerprints from a fairly typical layer grown in Würzburg, albeit one with a relatively large domain wall nucleation propagation energy. To illustrate the

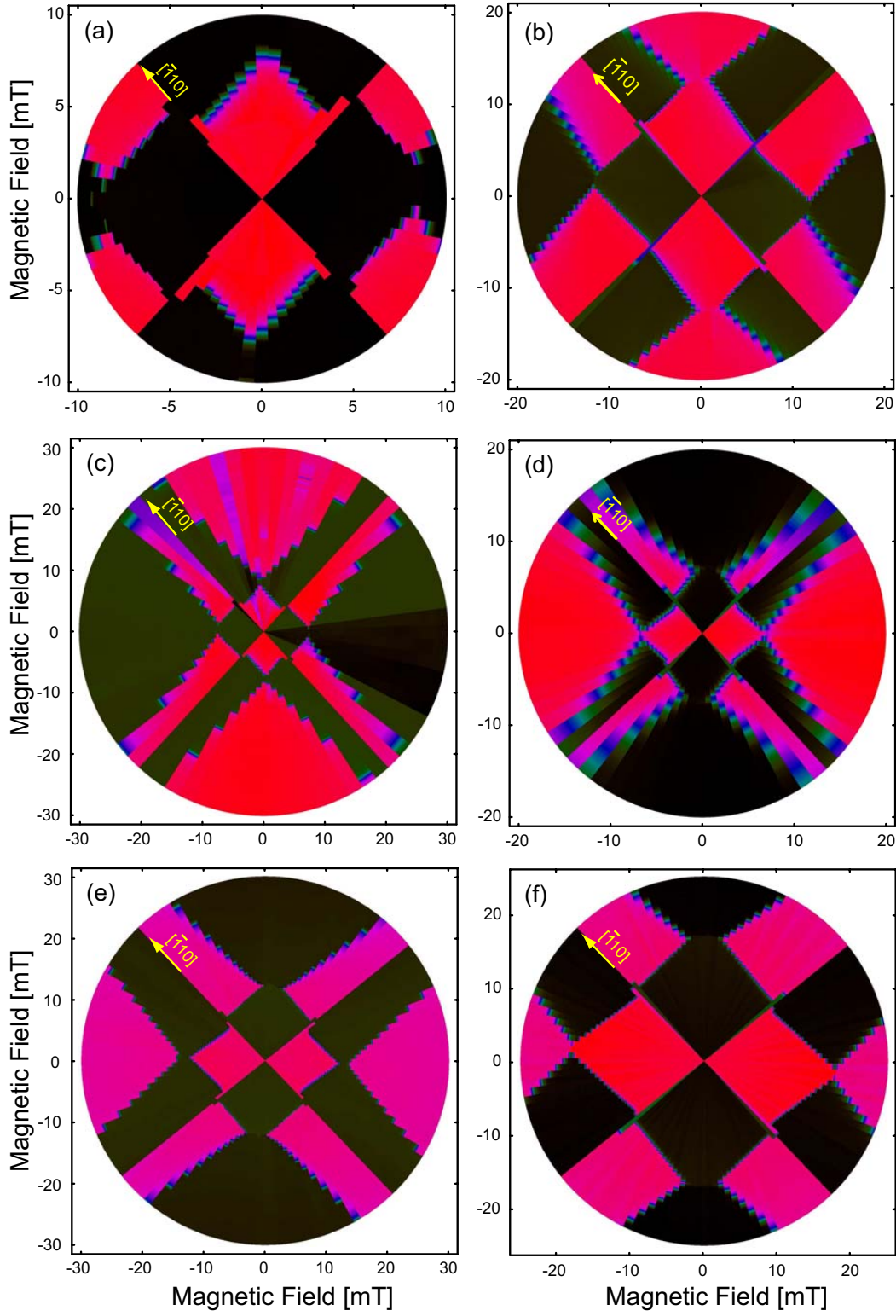


Figure 6. Fingerprints from $(\text{Ga},\text{Mn})\text{As}$ layers grown in various laboratories. a) and b) are layers grown in Würzburg with strong $[010]$ and $[110]$ easy axis, respectively. The other fingerprints are from layers grown at c) IMEC, d) Nottingham, e) Tohoku, and f) Notre Dame.

	$\epsilon/M(\text{mT})$	$K_{110}/K_{biax}(\%)$	$K_{010}/M(\text{mT})$
Wü. from Fig. 4	18	18	1.0
Wü. with large [010]	8.5	7	1.4
Wü. with large [110]	12	21	0.7
IMEC	7.8	11	0.7
Nottingham	7.1	9	0.65
Tohoku	12	4	1.25
Notre-Dame	16	9	0.75

Table 1. Characterization parameters extracted from the anisotropy fingerprints on various layers.

typical spread that can be expected, we present in Fig. 6 two additional Würzburg layers with rather pronounced [010] (Fig. 6a) or [110] (Fig. 6b) components. In parts c-f of the figure we compare these to fingerprints on layers grown at IMEC, Nottingham, Tohoku, and Notre Dame. Values of the various parameters extracted from all these layers are given in Table 1. The figure illustrates that not only the amplitude, but also the sign of the two uniaxial components can vary between samples. For the [110] uniaxial, this change in sign can be seen by a 90° rotation of the long axis of the rectangle, whereas the sign of the [010] is determined by whether the quarter of the rectangle with its primary diagonal along [010] is larger or smaller than that with the diagonal along [100]. Note that the sign of the color scale (determining which regions are red and which are black) is determined by the direction of the current flow during the measurement, and is irrelevant to the current investigation.

As is clear from the table, all samples show a significant contribution of both a [110] and [010] uniaxial anisotropy component. The values of the parameters that can be extracted from the fingerprints show variance from sample to sample, and typically fall in the range of some 7 to 18 mT for ϵ/M , 0.6 to 1.5 mT for K_{010}/M , 4 to 20% for the ratio of K_{110}/K_{biax} . Note that while the fingerprint technique cannot be used to reliably extract exact values for K_{biax} , the shape of the curve as the magnetization rotates away from the easy axis towards the external magnetic field at higher fields can be used to estimate the strength of K_{biax}/M . All samples investigated showed a value of approximately 100 mT for this parameter which means that the values of K_{110}/K_{biax} quoted in percent in the table are also estimates of K_{110}/M in mT.

While the table clearly shows significant variation from sample to sample, it nevertheless allows the extraction of useful rules of thumb for relative amplitude of the various terms. As a general statement, the ratio of $K_{biax} : K_{110} : K_{010}$ is of order 100 : 10 : 1, and the domain wall nucleation/propagation energy is of the order of 10% of the biaxial anisotropy constant.

The range of values for K_{010}/M and ϵ/M seen in the samples discussed in this study is a fair representation of (Ga,Mn)As in general. The span of values for the K_{110}/K_{biax}

ratio, which is already in the table larger than the other parameters, is however only a reflection of the subset of samples that we investigated. In general, this ratio can easily be tuned over a much larger range, for example as a function of hole concentration [4] or of temperature [11]. No systematic distinction is observed between samples from various source.

5. Conclusions

In conclusion, we have used the anisotropy fingerprint technique to analyze the magnetic anisotropy properties of multiple (Ga,Mn)As layers. We have shown that this technique is a reliable means of characterizing a given layer, and that it can be used as a quality control check of the growth. Moreover, we have examined pieces of (Ga,Mn)As grown in various laboratories around the world, and found that all samples exhibit three magnetic anisotropy components: A biaxial anisotropy along ([100] and [010]), a uniaxial along [110] (or $\bar{1}\bar{1}0$) and a second uniaxial along either [100] (or [010]), showing that the existence of all three terms is an inherent property of (Ga,Mn)As, and that it is only the relative strength of the terms which varies from sample to sample. As a rough rule of thumb, the ration of the biaxial anisotropy, the [110] uniaxial and the [010] uniaxial is of order 100 : 10 : 1.

Acknowledgements

The authors wish to thank S. Hümpfner and V. Hock for sample preparation, and acknowledge the financial support from the EU (NANOSPIN FP6-IST-015728) and the National Science Foundation (US) Grant DMR06-03752.

References

- [1] F. Matsukura, M. Sawicki, T. Dietl, D. Chiba, and H. Ohno, *Physica E* **21**, 1032 (2004).
- [2] X. Liu, Y. Sasaki, and J. K. Furdyna, *Phys. Rev. B* **67**, 205204 (2003).
- [3] M. Sawicki, F. Matsukura, A. Idziaszek, T. Dietl, G. M. Schott, C. Rueter, C. Gould, G. Karczewski, G. Schmidt, and L. W. Molenkamp, *Phys. Rev. B* **70**, 245325 (2004).
- [4] M. Sawicki, K. Y. Wang, K. Edmonds, R. Campion, C. Staddon, N. Farley, C. Foxon, E. Papis, E. Kamiska, A. Piotrowska, T. Dietl, and B. Gallagher, *Phys. Rev. B* **71**, R121302 (2005).
- [5] H. X. Tang, R. K. Kawakami, D. D. Awschalom, and M. L. Roukes, *Phys. Rev. Lett.* **90**, 107201 (2003).
- [6] C. Gould, C. Rüster, T. Jungwirth, E. Girgis, G. M. Schott, R. Giraud, K. Brunner, G. Schmidt, and L. W. Molenkamp, *Phys. Rev. Lett.* **93**, 117203 (2004).
- [7] J. Furdyna, X. Liu, N. Lim, Y. Sasaki, T. Wojtowicz, and I. Kuryliszyn, *Journ. Korean Phys. Soc* **S579**, 2003 (42).
- [8] R. Campion, K. Edmonds, L. Zhao, K. Wang, C. Foxon, B. Gallagher, and C. Staddon, *Journ. Cryst. Growth* **247**, 20 (2003).
- [9] G. Schott, G. Schmidt, G. Karczewski, L.W.Molenkamp, R. Jakiela, and A. Barcz, *Appl. Phys. Lett.* **82**, 4678 (2003).
- [10] K. Pappert, S. Hümpfner, J. Wenisch, K. Brunner, C. Gould, G. Schmidt, and L. W. Molenkamp, *Appl. Phys. Lett.* **90**, 062109 (2007).

- [11] K. Pappert, C. Gould, M. Sawicki, J. Wenisch, K. Brunner, G. Schmidt, and L. W. Molenkamp, New Journ. Phys. **9**, 354 (2007).
- [12] D. V. Baxter, D. Ruzmetov, J. Scherschligt, Y. Sasaki, X. Liu, J. K. Furdyna, and C. H. Mielke, Phys. Rev. B **65**, 212407 (2002).
- [13] J. P. Jan, *Solid State Physics* ((Eds: F. Seitz, D. Turnbull), Academic Press Inc., New York, 1957), pp. Vol. 5, p.1.
- [14] T. McGuire and R. Potter, IEEE Trans. Magn. **MAG-11**, 1018 (1975).
- [15] A. W. Rushforth, K. Vyborny, C. S. King, K. W. Edmonds, R. P. Campion, C. T. Foxon, J. Wunderlich, A. C. Irvine, P. Vasek, V. Novak, K. Olejnk, J. Sinova, T. Jungwirth, and B. L. Gallagher, Phys. Rev. Lett. **99**, 147207 (2007).
- [16] U. Welp, V. Vlasko-Vlasov, X. Liu, J. Furdyna, and T. Wojtowicz, Phys. Rev. Lett. **90**, 167206 (2003).
- [17] S. T. B. Goennenwein, S. Russo, A. F. Morpurgo, T. M. Klappwijk, W. van Roy, and J. de Boeck, Phys. Rev. B **71**, 193306 (2005).